ISTITUTO NAZIONALE DI FISICA NUCLEARE

Sezione di Genova

INFN/BE-82/3
2 Novembre 1982

E. Di Salvo:

EVIDENCE FOR SURFACE WAVES AND REFLECTION IN $^{16}O+^{28}Si$ ELASTIC SCATTERING

Servizio Documentazione
dei Laboratori Nazionali di Frascati

INFN - Istituto Nazionale di Fisica Nucleare
Sezione di Genova

INFN/BE-82/3
2 Novembre 1982

EVIDENCE FOR SURFACE WAVES AND REFLECTION IN $^{16}O + ^{28}Si$ ELASTIC SCATTERING

E. Di Salvo
Istituto Nazionale di Fisica Nucleare, Sezione di Genova and
Istituto di Scienze Fisiche dell'Università di Genova

ABSTRACT

A surface wave model is proposed for interpreting the elastic scattering of ^{28}Si on ^{16}O. The surface waves are excited at the surface of the nuclear-interaction region and propagate along it, they are focused at forward and at backward. At large angles the surface rays interfere with the reflected rays; on the contrary, at small angles they interfere with the Coulomb refracted rays, producing the typical Fresnel diffraction pattern. We make fits to the experimental data both at fixed energies and at a fixed angle ($\theta = 180°$); we also discuss the consistency among the various parameters found; moreover we extract a value of the nuclear-interaction radius.

RIASSUNTO

Si propone un modello ad onde superficali per interpretare la diffusione elastica di ^{28}Si su ^{16}O. Queste onde sono eccitate alla superficie della regione d'interazione nucleare e si propagano attorno ad essa, infine sono focalizzate nella direzione in avanti ed all'indietro. A grandi angoli i raggi superficali interferiscono con i raggi riflessi, a piccoli angoli, invece, interferiscono con i raggi che risentono della sola azione Coulombiana: in tal modo si ha la tipica diffrazione alla Fresnel. Si approssimano i dati sperimentali ad energie fissate ed anche ad angolo fissato ($\theta = 180°$); si discute la compatibilità tra i vari parametri trovati nei fit; inoltre si estrae un valore del raggio d'interazione nucleare.

1. - INTRODUCTION

A surface wave model has been proposed[1], in order to explain the anomalous large angle scattering (ALAS) of alpha particles on nuclei like ^{16}O, ^{28}Si and ^{40}Ca. Now the elastic scattering of $^{16}O+^{28}Si$ exhibits, near the backward direction, some features which are very similar to those observed in ALAS of α-Nuclei elastic collisions, i.e.:

a) the angular distribution presents a strong oscillatory large angle peak, which is "anomalous" with respect to the usual behaviour of the backward differential cross sections;

b) the backward excitation function has an oscillatory trend, with an envelope which decreases with energy;

c) an isotope effect is observed, in the sense that the large angle elastic scattering cross section between Oxygen and Silicon isotopes, like $^{18}O + ^{28}Si$ or $^{16}O + ^{29}Si$, is considerably smaller than the corresponding $^{16}O + ^{28}Si$ cross section.

Therefore it seems quite natural to try to extend the surface wave model to $^{16}O + ^{28}Si$ elastic scattering. This model presents some analogies with the one elaborated by Fuller and Moffa[2]: however the formalism used and the mathematical process adopted are quite different.

Previously, some authors tried to explain ALAS in $^{16}O + ^{28}Si$ by various mechanisms, like shape resonances[3], a parity-dependent potential[4,5] or by an optical potential whose imaginary part has a radius smaller than the real one[6,7].

In this work we shall use concepts like reflection, refraction or diffraction, referring to particle trajectories rather than to light rays. This approach allows us to introduce a parametrization which does not depend on the specific form of the nuclear potential. We use the same formalism that has been developed in the paper[1], which, hereafter, will be referred to as I. However, due to the stronger Coulomb interaction, the differential cross section in the forward half-space presents a fundamental difference with respect to the angular distribution of α-nuclei elastic scattering. As pointed out by Frahn[8], the Coulomb interaction deflectes the particles in such a way that those which are grazing to the nuclear interaction region appear to be esmitted from a point-like source set at a finite distance from the centre of mass. A "Coulomb region" of finite angular size is produced behind the nuclear interaction sphere: the diffracted rays, which propagate into this region, are focalized at forwards and interfere with the Coulomb refracted rays. If the Sommerfeld parameter is small (e.g. in the case of α-^{40}Ca we have $\eta \simeq 2$), the angular size of the "Coulomb" region is small and the interference among the rays is strong, it produces the typical Fraunhofer-like diffraction pattern. But for values of the Sommerfeld parameter of the order of 10 (as is the case of $^{16}O + ^{28}Si$) or larger, the interference of the diffracted and Coulomb refracted rays is weaker and produces a Fresnel-like diffraction pattern, which is typical of the light from a source posed at a finite distance from the obstacle. Now, unlike the Fraunhofer pattern, the Fresnel diffraction can be described simply in terms of the amplitudes of the diffracted rays and the Coulomb refracted rays. Therefore we shall interpret the differential cross section by means of the surface rays which interfere, at small angles, with the Coulomb refracted rays and, at large angles, with the reflected rays. As far as these last are concerned, from our phenomenological analysis it results that the nuclear potential is more reflecting, and therefore sharper than the usual Woods-Saxon potential employed in the literature.

Let us recall the assumptions of our model.

a) The scattering process between the two ions is approximated by the diffusion of a point-like particle by a sphere having the dimensions of the nuclear interaction region.

b) The sphere is assumed to have an opaque core surrounded by a nearly transparent shell.

c) The conditions for a quasi-classical approximation are supposed to be realized, i.e. one assumes[9] that

$$k R \gg 1 \qquad \text{and} \qquad \hbar^2 k \ll \mu R \overline{V}$$

where k is the wavenumber in the c.m.s., R the radius of the nuclear interaction sphere, μ the reduced mass and $\overline{V}$ the mean value of the potential inside the sphere.

d) The potential between ^{16}O and ^{28}Si is assumed to vary rapidly near the boundary of the nuclear interaction region. Moreover the absorptive region is supposed not to cause any appreaciable reflection nor surface waves at the interior of the transparent shell.

The paper is organized as follows. In Sect. 2. we give an outline of the theory developed in I. In Sect. 3. we present the results of our phenomenological analysis. In Sect. 4. we draw some conclusions.

2. - OUTLINE OF THE THEORY

We assume a potential of the form (see I, formulas (3a) and (3b))

$$U(R)= \begin{cases} V_c(r) + V_n(r) \quad , & r \leq R, \qquad (1a) \\ \dfrac{2\eta}{kr} E \quad , & r > R, \qquad (1b) \end{cases}$$

where

$$\eta = \frac{\mu Z Z' e^2}{\hbar^2 k}$$

is the Sommerfeld parameter and V_n is the complex-valued nuclear potential, whereas $V_c(r)$ is the electrostatic potential inside the nuclear interaction sphere. In the short wavelength approximation we assume that the wavefunction can be written as a sum od terms like $A\, e^{i\Phi}$. Substituting in the Schrödinger equation, we get, in the limit of large values of k, the eikonal and the transport equation, i.e.

$$(\vec{\nabla}\Phi)^2 = n^2 k^2 , \qquad (2)$$

$$\vec{\nabla}\cdot(A^2 \vec{\nabla}\Phi) = 0 , \qquad (3)$$

where

$$n^2 = 1 - \frac{U(r)}{E}$$

This approximation fails at the boundary of the nuclear sphere, where we assumed the potential to vary rapidly with respect to the Broglie wavelength. Now we can reasonably conjecture that, on the boundary, phonomena like reflection, refraction and diffraction occur, similarly to the case of a discontinuous potential.

In the following we review briefly the theory which we have developed in I: firstly we determine the behaviour of the trajectories at large distance from the scattering centre; then we give the results that we found in the preceding paper, as regards the scattering amplitude and the differential cross section.

2.1. - Ray tracing

As we saw in I, the trajectory is tangent to the nuclear interaction sphere when the angular momentum λ assumes the value

$$\lambda = \lambda_g = k R \sqrt{1 - \frac{2\eta}{kR}} \qquad (4)$$

Therefore, for $\lambda > \lambda_g$, the trajectory does not meet the sphere and undergoes a pure Coulomb deflection. On the contrary, when $\lambda < \lambda_g$, the trajectory hits the boundary of the sphere, where it split into a reflected and a refracted trajectory. Now we make the simplifying assumption that the opaque core absorbs all the refracted rays - except the limiting refracted ones - so that we do not worry about them.

Lastly, when $\lambda = \lambda_g$, the grazing trajectory splits at the point of tangency into there branches: one leaves the sphere tangentially, another a limiting refraction and the third describes an arc geodesic on the surface of the sphere; this last is named surface ray and undergoes at each point the same splitting that it had at the point of tangency. The limiting refracted ray describes a shortcut across the trasparent shell and splits again when it reaches the surface.

Now, in order to determine the differential cross section, we have to examine the behavior of the trajectories at very large distances from the nuclear interaction sphere. The grazing trajectory - more precisely the branch which leaves the surface of the sphere tangentially - points, at large distance, in the direction

$$\theta = \theta_g = 2 \operatorname{arctg} \frac{\eta}{\lambda_g} \ . \tag{5}$$

A particle with angular momentum greater than λ_g undergoes only the Coulomb action and therefore is scattered in a direction

$$\theta = 2 \operatorname{arctg} \frac{\eta}{\lambda} < \theta_g \ ; \tag{6}$$

(c.f.r. I, formula (27)).

On the other hand a trajectory with angular momentum less than λ_g undergoes reflection at the surface of the sphere and is scattered in a direction θ such that

$$\cos \frac{\theta}{2} = \sin (\overline{\theta}_i - \overline{\theta}_c) \ , \tag{7}$$

where

$$\overline{\theta}_i = \operatorname{arc\,sin} \frac{\eta \ kR + \lambda^2}{kR(\lambda^2 + \eta^2)^{1/2}} \tag{8}$$

and

$$\overline{\theta}_c = \operatorname{arc\,sin} \frac{\eta}{(\lambda^2 + \eta^2)^{1/2}} \tag{9}$$

(c.f.r. I, formula (37)). In this case one can see that $\theta > \theta_g$. The diffracted rays - either those which describe a simple arc of geodesic or those which take also one or more shortcuts - are scattered at every angle.

Moreover, we have to take into account those rays which are critically refracted at the point of tangency with the nuclear interaction sphere and take one or more shortcuts and lastly, without describing any arc of geodesic, emerge in a direction

$$\theta_p = \left| p \, \theta_t - \theta_g \right| \quad (\mathrm{mod}\pi), \ (0 < \theta_p < \pi). \tag{10}$$

2.2. - Scattering Amplitude and differential Cross Section

The wavefunction - and therefore the scattering amplitude - consists in a sum of terms, each of which

represents the contribution of a single trajectory. Therefore from the ray tracing it follows that

$$f(\theta) = f_c(\theta) + f_d(\theta), \quad (\theta < \theta_g), \tag{11a}$$

$$f(\theta) = f_r(\theta) + f_d(\theta), \quad (\theta > \theta_g), \tag{11b}$$

where $f_c(\theta)$ is the contribution from pure Coulomb trajectories, $f_r(\theta)$ the contribution from direct reflection and $f_d(\theta)$ the contribution from the diffraction. Now we recall the expressions of $f_c(\theta)$, $f_r(\theta)$ and $f_d(\theta)$ that we deduced in I, referring to that paper as regards the notations used. We have

$$f_c(k, \theta) = \frac{\eta}{2\, i\, k\, R \sin^2 \frac{\theta}{2}} \; e^{2i\eta\left(\log \frac{\eta}{\sin \frac{\theta}{2}} - 1\right)} \; ; \tag{12}$$

$$f_d(k, \theta) = \sum_{p=0}^{P} \left[f_d^{(p)+}(k, \theta) + f_d^{(p)-}(k, \theta) \right] , \tag{13}$$

where

$$f_d^{(p)\pm}(k, \theta) = \frac{i^{n_p^{\pm}} e^{ip\phi_s} e^{2i\Delta_g} \mathcal{L}_p(\zeta_p^{\pm})}{\left[\sin\theta \cos(\frac{1}{2}\theta_g) \right]^{1/2}} \sum_{n=1}^{\infty} D_n D'_n \; e^{i\lambda_n \zeta_p^{\pm}} \tag{14}$$

and

$$\zeta_p^{\pm} = \pm\theta + \theta_g - p\,\theta_t \pmod{2\pi} \; , \quad 0 < \zeta_p^{\pm} \leq 2\pi, \tag{15}$$

$$\Delta_g = \eta \left[\log(k\, R - \eta) - 1 \right] \; ; \tag{16}$$

lastly ϕ_s and $\mathcal{L}_p(\zeta_p^{\pm})$ are defined in I, formulas (54) and (59) respectively. $n_p^{\pm}$ depend on the number of focal points crossed by the counterclockwise and clockwise travelling rays.

As regards the reflection amplitude, we have

$$f_r(k, \theta) = \frac{1}{2} \frac{R_v}{R} \left[F(\theta) \right]^{-\frac{1}{2}} e^{2i\Delta_r} \; \mathcal{R}(\theta), \tag{17}$$

where $F(\theta)$ is given by formula (65) of I, while

$$\Delta_r = \eta \left[\log\left(\sqrt{\lambda_g^2 - \lambda_r^2} + k\, R_v - \eta \right) - 1 \right] - \sqrt{\lambda_g^2 - \lambda_r^2} \tag{18}$$

and λ_r is the angular momentum of the reflected trajectory: it can be expressed as a function of θ by inverting formulas (7), (8) and (9). We have introduced a new quantity, R_v, which is the average radius of the nuclear interaction region, to be distinguished from R, which is the maximum distance from the scattering centre at which the nuclear interaction has some influence. In this connection let us specify that the factor $F(\theta)$, whose expression is given by formula (65) of I, is to be calculated using R_v in place of R. Lastly the formula of the reflection coefficient $\mathcal{R}(\theta)$ will be discussed in detail in the following section.

In the expression (14) of the diffracted ray contribution we have summed over all the possible "modes": each "mode" is characterized by diffraction coefficients D_n and D'_n (n=1, 2, ...) and by a decay exponent α_n, such that

$$\lambda_n = \lambda_g + i\alpha_n \,. \tag{19}$$

The energy dependence of D_n, D'_n and α_n will be discussed in the next section. When $\zeta_p^{\pm}$ is sufficiently large, we may take into account only the "mode" for which the (complex) angular momentum λ_n has the smallest imaginary part: if we denote with $\lambda=\lambda_1$ this value of the angular momentum, $f_d(k, \theta)$ reduces to the expression given in I, formula (60).

The scattering amplitude (11a) or (11b) fails in certain angular regions centred on the angles θ_p given by furmula (10): in these angular intervals, which we call transition regions (see (10)), the contribution of the limiting reflected rays ($\theta = \theta_g$) or limiting refracted rays is to be taken account; moreover in these regions all the excitation modes must be considered. Here the ray approximation does not apply, since the interference effects are too strong. As we shall see in the phenomenological analysis, we assume that the surface rays taking more than one shortcut give a negligible contribution. Then, we have two transition regions in correspondence to θ_g and to $\theta_t - \theta_g$. Therefore, if we restrict ourselves at angles sufficiently at forward or at back ward, the transition regions do not concern us.

With the above approximations in mind, we study the formula of the scattering amplitude at small angles ($\theta < \theta_g$) and near the backward direction.

i) Let us consider the scattering amplitude for θ near to π. Since the surface rays take at most one shortcut, ζ_0^+ and ζ_1^+ are sufficiently large, and we can replace the sum over the modes by the term corresponding to n=1; moreover we may neglect the angular dependence in the polynomial $\mathcal{L}_1(\zeta_1^{\pm})$. Since in this case $n_p^- = n_p^+ - 1$, we have

$$f_d(k, \theta) \simeq \frac{D_1 D'_1 \, e^{i(2\Delta_g - \frac{\pi}{4})} \sqrt{2\pi\lambda_g}}{\left[\cos(\tfrac{1}{2}\theta_g)\right]^{1/2}} \left[\sum_{p=0} e^{ip\phi_s} \, i^{n_p^+} \, e^{i\lambda_1 \nu_p} \, \mathcal{L}_p(\nu_p) \right] \cdot$$

$$\frac{e^{i\left[\lambda_1(\pi-\theta) - \frac{\pi}{4}\right]} + e^{-i\left[\lambda_1(\pi-\theta) - \frac{\pi}{4}\right]}}{(2\pi\lambda_g \sin\theta)^{1/2}} \,, \tag{20}$$

where

$$\nu_p = \pi - p\,\theta_t + \theta_g \qquad (\mathrm{mod}\ 2\pi), \qquad 0 < \nu_p \leq 2\pi$$

and D_1 and D'_1 are the diffraction coefficients corresponding to the "mode" n=1. For $\theta \to \pi$ the focusing effect, due to the presence of an axial caustic, is to be taken into account. As we have shown in I, the correct behaviour near and at the caustic can be obtained replacing the last factor in (20) with the Legendre function $P_{\lambda_1 - \frac{1}{2}}(-\cos\theta)$.

Now, in order to write the differential cross section, we recall that we have defined a dimensionless scattering amplitude, such that (see I)

$$\frac{d\sigma}{d\Omega} = R^2 \left| f(\theta) \right|^2 \tag{21}$$

For θ near to π, substituting (17) and (20) into (11b) and taking into account the focusing effect, we get

$$\frac{d\sigma}{d\Omega} \approx R^2 \left| A e^{i\psi} P_{\lambda_1 - \frac{1}{2}}(-\cos\theta) + \frac{1}{2} \frac{R_v}{R} e^{2i\Delta_r(k,\theta)} R(\theta) \left[F(\theta)\right]^{-1/2} \right|^2, \tag{22}$$

where A and ψ are real functions such that

$$A e^{i\psi} = \frac{D_1 D_1' e^{i(2\Delta_g - \frac{\pi}{4})} (2\pi\lambda_g)^{1/2}}{(\cos\frac{1}{2}\theta_g)^{1/2}} \sum_{p=0}^{1} e^{ip\psi_s} e^{i\lambda_1 \nu} P_{\mathcal{L}_p}(\nu_p)\, i^{n_p^+}. \tag{23}$$

ii) Now let us turn our attention to the scattering amplitude for θ near to 0. In this case we neglect the contribution corresponding to one shortcut, since the corresponding surface ray has to describe an arc $\zeta_1^+ = 2\pi \pm \theta - \theta_t + \theta_g$ and therefore is largely damped. Moreover in this angular region $n_o^+ = -1$, $n_o^- = 0$. Then, from (14) we get

$$f_d(k,\theta) = \frac{e^{i(2\Delta_g - \frac{\pi}{4})}}{\left[\cos(\frac{1}{2}\theta_g)\sin\theta\right]^{1/2}} \sum_{n=1}^{\infty} e^{i\lambda_n \theta_g} D_n D_n' \left[e^{i(\lambda_n \theta - \frac{\pi}{4})} + e^{-i(\lambda_n \theta - \frac{\pi}{4})} \right]. \tag{24}$$

At $\theta = 0$ there is the axial caustic and we could take into account the focalizing effect by suitably transforming formula (24), as we did at backward. However, for the moment we are not interested in such a modification. Rather, if we restrict ourselves to angles such that $\theta > (\text{Im}\,\lambda_1)^{-1}$, we can approximate (24) by

$$f_d(k,\theta) \simeq \frac{e^{2i\Delta_g}}{(\cos\frac{1}{2}\theta_g \sin\theta)^{1/2}} e^{i\lambda_g(\theta_g - \theta)} \sum_{n=1}^{\infty} D_n D_n' e^{-\alpha_n(\theta_g - \theta)}. \tag{25}$$

The approximation fails in a neighborhood of $\theta = \theta_g$, where we have a transition region. The series in (25) converges for $\theta \leq \theta_g - \varepsilon$ for every $\varepsilon > 0$, the rapidity of convergence depending on $\theta_g - \theta$.

Formula (25) is not suitable for a phenomenological analysis, since it contains a too large number of parameters. In the following section we shall show the amplitude (25) may be approximated, uniformly in a neighborhood of $\theta = 0$, by the formula

$$f_d(k,\theta) \simeq C\sqrt{2\pi\lambda_g}\, \frac{e^{-i\frac{\pi}{4}} e^{2i\Delta_g} e^{i\lambda_a \theta_g}}{(\cos\frac{1}{2}\theta_g)^{1/2}} P_{\lambda_a - \frac{1}{2}}(\cos\theta), \tag{26}$$

where $\lambda_a = \lambda_g + i\alpha_a$ and C and α_a are complex constants to be defined in the following section. Then the cross section at angles $\theta < \theta_g$ is given by

$$\frac{d\sigma}{d\Omega} \approx R^2 \left| B e^{i\gamma} P_{\lambda_a - \frac{1}{2}}(\cos\theta) + f_c(k,\theta) \right|^2, \tag{27}$$

where $f_c(k,\theta)$ is given by (12) and

$$B e^{i\gamma} = C e^{i(-\frac{\pi}{4}+2\Delta_g)} e^{i\lambda_n \theta_g} \left(\frac{2\pi\lambda_g}{\cos\frac{1}{2}\theta_g}\right)^{1/2} \tag{28}$$

Formula (27) has been used also by Fuller and Moffa[2], in order to describe the differential cross section at small angles, in some cases of heavy ion elastic scattering.

3. - PHONOMENOLOGICAL ANALYSIS

In this section we use the preceding formulas to fit the experimental data of $^{16}O+^{28}Si$ elastic scattering: we consider the large angle and small angle differential cross section in an energgy interval between 21 and 35 MeV in the c.m. s. (see experimental data of Braun-Munzinger et al.[11]. At large angles we fit both the angular distributions at six different energies and the excitation function at backward; to this end, we have to specify the angular and energy dependence of the reflection coefficient and the energy dependence of the decay exponents α_n and of the diffraction coefficients D_n, D'_n. On the other hand, at small angles we have to justify the approximation (26), which allows us to use formula (27) in the fixed energy fits.

3.1. - Large Angle Differential Cross Section

Let us consider firstly the fixed energy fits. We try to interpret the angular distributions taking into account the sole surface wave effect, so that formula (22) reduces to

$$\frac{d\sigma}{d\Omega} = N \left| P_{\lambda_1 - \frac{1}{2}}(-\cos\theta) \right|^2 , \tag{29}$$

where

$$N = R^2 A^2 .$$

We fit the data using N, Re λ_1, Im λ_1 as free parameters. Only the fit at E_{CM}=34.8 MeV is satisfactory (see Fig. 1); at lower energies, one can see a discrepancy between the experimental data and the theoretical curves: the

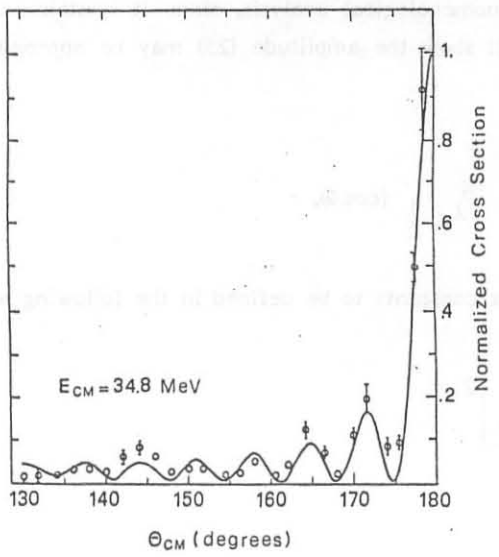

FIG. 1

discrepancy tends to decrease towards increasing energies. This fact suggests that a reflection contribution should be taken into account. We assume a phonomenological reflection coefficient from a Woods-Saxon barrier, i.e. (see I and ref. (12)):

$$\mathcal{R}(\theta) = \frac{\Gamma(2i\Delta k_r)\Gamma\left[-i\Delta(K_r+k_r)\right]\Gamma\left[1-i\Delta(K_r+k_r)\right]}{\Gamma(-2i\Delta k_r)\Gamma\left[-i\Delta(K_r-k_r)\right]\Gamma\left[1-i\Delta(K_r-k_r)\right]} , \tag{30}$$

where Δ is the diffuseness parameter and

$$k_r = \left[k^2\left(1 - \frac{2\eta}{k R_v}\right) - \frac{\lambda_r^2}{R_v}\right]^{1/2} , \tag{31}$$

$$K_r = \left[k_r^2 + 2\mu \hbar^{-2} V_o\right]^{1/2} ; \tag{32}$$

V_o is the depth of the barrier, μ the reduced mass, R_v and λ_r have been defined in formulas (17) and (18). Note that we do not necessary assume a Woods-Saxon potential, but we merely take into account a contribution of reflection from a nuclear potential with a given diffuseness Δ.

We fit the sets at E_{CM}=21.1, 22.7, 24.3, 26.2 and 31.6 MeV by formula (22), using for $\mathcal{R}(\theta)$ the expression (30). For each set we use A, ψ, Re λ_1, Im λ_1 as free parameters. We give R_v and v_o the values of the parameters corresponding to the potential D23 reported in Ref. (13): this potential seems to be the most suitable for describing the large angle behaviour of the angular distribution of $^{16}O+^{28}Si$, since its imaginary part has a radius smaller than the real part. So R_v=7.946 fermi, V_o=5 MeV are the values reported. The diffuseness is left as a free parameter, but independent of energy. The results of the fits are shown in Fig. 2b. The fit parameters A, ψ, Re λ_1 and Im λ_1 are reported in Table I. The diffuseness is found to be 0.30 fermi: it seems to be somewhat low with respect to the commonly reported values of Δ, but it is in agreement with the value obtained by Dehnhard et al.[4] for the imaginary part of the nuclear potential.

TABLE I - Values of the fit parameters, as obtained from the large angle fits to the $^{16}O+^{28}Si$ elastic scattering data at fixed energies: column a refers to the fits where only the surface ray contribution is considered; column b refers to the fits where the interference with the reflected rays is taken into account.

E_{cm}	$R \cdot A\left[(mb/sr)^{\frac{1}{2}}\right]$		Re λ_1		Im λ_1		ψ	θ_{min} (deg)	χ^2	
(MeV)	a	b	a	b	a	b			a	b
21.1	1.594	1.255	8.05	11.78	1.794	1.262	1.075	138.1	588	25
22.7	1.139	1.767	11.77	14.23	1.388	.667	.210	137.	827	22
24.3	1.837	1.915	16.14	16.83	.729	.996	-1.080	145.5	181	67
26.2	1.287	1.282	17.41	17.92	.583	.930	-4.785	153.8	57	20
31.6	.638	.662	22.00	22.11	1.516	1.223	-6.900	155.8	60	52
34.8	.401		26.30		.748			130.	133	

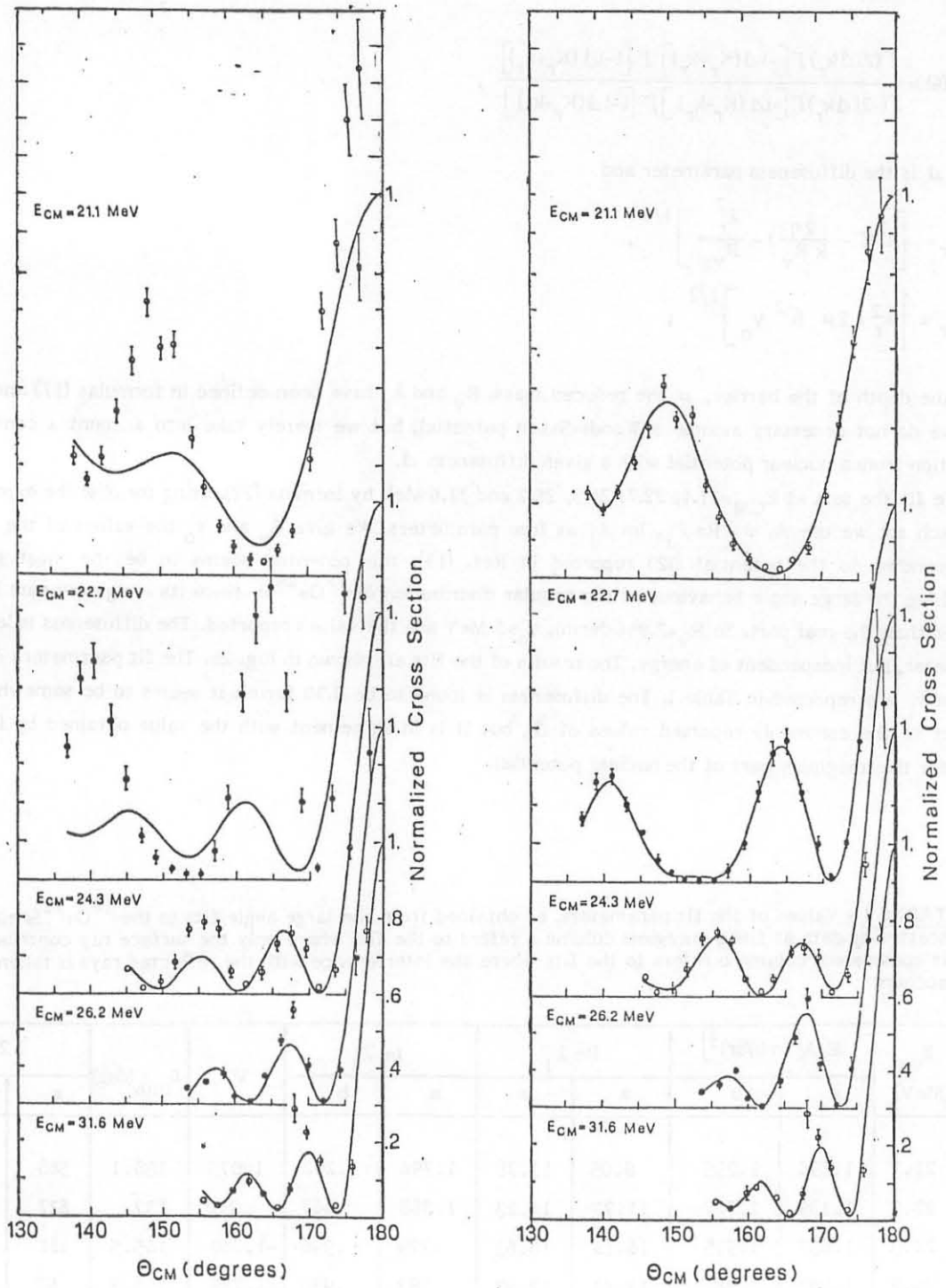
E_CM = 21.1 MeV
E_CM = 22.7 MeV
E_CM = 24.3 MeV
E_CM = 26.2 MeV
E_CM = 31.6 MeV
Normalized Cross Section
Θ_CM (degrees)
130
140
150
160
170
180

FIG. 2

Let us note that formula (22) has been deduced for values of θ near π and the angular dependence of $\mathscr{L}_1(\zeta_1)$ has been neglected, as well as all the modes corresponding to n > 1. Forcing a little bit the mathematics, we have used that formula for a larger angular range, extending out fits as long as the agreement with the data is satisfactory. In this connection we observe that the angular region to which the fits can be extended varies from set to set and is greatest at the highest energy; a similar trend has been noted also in α-^{40}Ca (see Γ). Below, when we discuss the excitation function, we shall give a tentative explanation of this fact.

Now let us turn attention to the energy dependence of the decay exponent and of the diffraction coefficients. To the first order in k^{-1} these quantities depend only on the local properties of the diffraction surface and on the incident field[14]. Of course, also the curvature of the incident trajectory should be taken into account; however, this effect could give rise to a complicated k-dependence, and, on the other hand, it could be too weak to be accounted for phenomenologically. In our phenomenological aoproach, we assume that the dependence of α_n, D_n, D'_n on the local wavenumber $k_c = \frac{1}{2}\lambda_g$ is the same as for a neutral sphere, i.e.:

$$\lambda_n = \lambda_g + (a_n + i\, b_n)\, \lambda_g^{1/3} \tag{33}$$

$$D_n D'_n = d_n\, \lambda_g^{-1/6} \tag{34}$$

Now we are able to study the energy dependence of the fit parameters and to fit the backward excitation function. As far as Re λ_1 is concerned, we fit the values reported in Table I approximating Re λ_1 by λ_g. The fit is shown in Fig. 3. We get the value R=9.07 fermi. As regards the excitation function, we use still formula (22), for $\theta = \pi$, together with (23). We assume that only the terms corresponding to p=0 (no shortcuts) and to p=1 (one

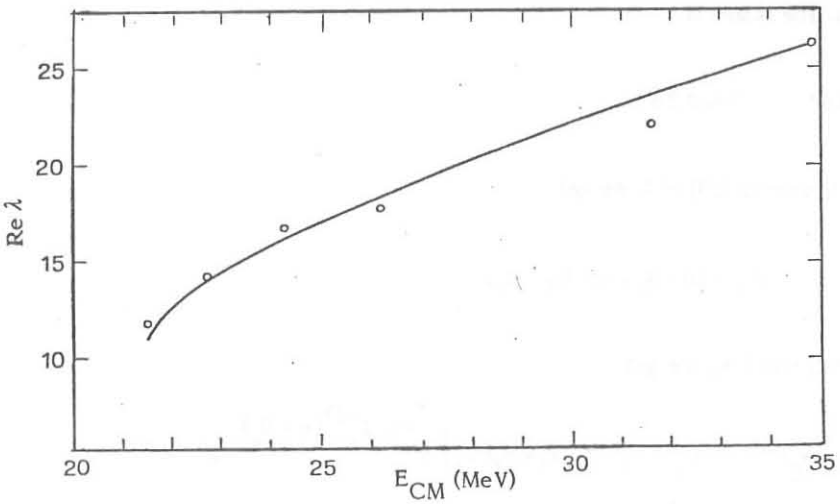

FIG. 3

shortcut) contribute to the scattering amplitude. We get

$$\left(\frac{d\sigma}{d\Omega}\right)_{\theta=\pi} = R^2 \left| A\, e^{i\psi} + \frac{1}{2}\frac{R_v}{R}\; e^{2i\Delta_r(k,\pi)}\; R(\pi) \left[F(\pi) \right] - \frac{1}{2} \right|^2 , \tag{35}$$

where

$$A = \frac{|D_1 D'_1|\, \sqrt{2\pi\lambda_g}}{(\cos\frac{1}{2}\theta_g)^{1/2}} \left| \mathscr{L}_o + \mathscr{L}_1 z \right| e^{-(\pi + \theta_g)\mathrm{Im}\,\lambda_1} \tag{36}$$

and

$$z = e^{i(\phi_s - \lambda_1 \theta_r - \frac{\pi}{2})} \tag{37}$$

We deduce the k-dependence of Im λ_1 and of ψ from the fixed energy fit parameters. As regards the phase ψ, we fit the five values reported in Table I by a linear function of k, getting

$$\psi = 39.25 - 11.85\ k. \tag{38}$$

As far as Im λ_1 is concerned, we fit the six values in Table I by formula (33); the result is

$$\text{Im}\ \lambda_1 = 0.364\ \lambda_g^{1/3} \tag{39}$$

Then we assume φ_s to be proportional to k, so that formula (37) reads as follows:

$$Z = e^{\text{Im}\ \lambda_1 \theta_t + i\varphi}, \tag{40}$$

where φ is a real function linearly dependent on k. In order to determine φ, we have fixed its values to π, 3π and 5π respectively in correspondence to three consecutive dipd of the excitation function. We have chosen the dips at sufficiently high energies, such that the reflection contribution is negligible, and we have determined φ by linear least squares. The result is

$$\varphi = 43.32\ k + 0.67 \qquad (\text{mod}\ 2\pi). \tag{41}$$

Taking into account formula (59) of I, we get

$$\mathcal{L}_o = 1; \qquad \mathcal{L}_1 = (\pi - \theta_t + \theta_g)\ D_{12}\ D_{21}\ . \tag{42}$$

Inserting (39) and (42) into (36), we get

$$A = \lambda_g^{1/3} (\cos \tfrac{1}{2} \theta_g)^{-1/2} \left| L_o + L_1 (\pi - \theta_t + \theta_g)\ z \right| e^{-b_1 \lambda_g^{1/3} (\pi + \theta_g)}, \tag{43}$$

where

$$b_1 = 0.364,$$

$$L_o = \left| \sqrt{2\pi}\ d_1 \right|,$$

$$L_1 = \sqrt{2\pi} \left| d_1\ D_{12}\ D_{21} \right|\ .$$

Now, if we insert (43) into (35) and take into account (38), (39), (40) and (41), we can fit the excitation function, using L_o, L_1 and θ_t as free parameters.

The fit is successful only for $E_{CM} < 26.$ MeV, whereas at higher energies the theoretical curve decreases more slowly than the experimental excitation function. Now it is reasonable to assume that the amplitude of the shortcut, which gives the main contribution to the differential cross section at backwards, is a decreasing function of the energy because of the increasing absorption by inelastic channels. Therefore we assume L_1 to be energy dependent and, in order to choose a suitable parametrization, we take a logarithmic plot of the excitation function versus the wave number k_{CM}, for $k_{CM} > k_o = 3.57$ fm^{-1}, which is the wave number corresponding to $E_{CM}=26.$ MeV. The logathmic plot suggests for L_1 a dependence of the type

$$\log L_1 = c + \mu\, k^{-\nu} \qquad (44)$$

where c, μ, ν, are positive constants. Then we do the fit to the excitation function up to $E_{CM}=31.5$ MeV, assuming

$$L_1(k) = \begin{cases} L_{10} & , \ (k \le k_o) \\ C \exp(\mu k^{-\nu}) & , \ (k > k_o) \end{cases}$$

with the constraint that $L_1(k)$ be continuous at $k=k_o$; so we take $L_{10}=C\exp(\mu k_o^{-\nu})$ and we use C, μ, ν, L_o and θ_t as free parameters. The fit is shown in Fig. 4. The values of the parameters resulting from the fit are

$\theta_t = 2.58$ rad

$R \cdot L_o = 0.84$ (mb/sr)$^{1/2}$

$$R \cdot L_1 = \begin{cases} 0.41 & (\text{mb/sr})^{1/2} \quad (k \le k_o) \\ 4.43 \exp(133.58\ k^{-2.662})\ 10^{-3} & (\text{mb/sr})^{1/2} \quad (k > k_o) \end{cases}$$

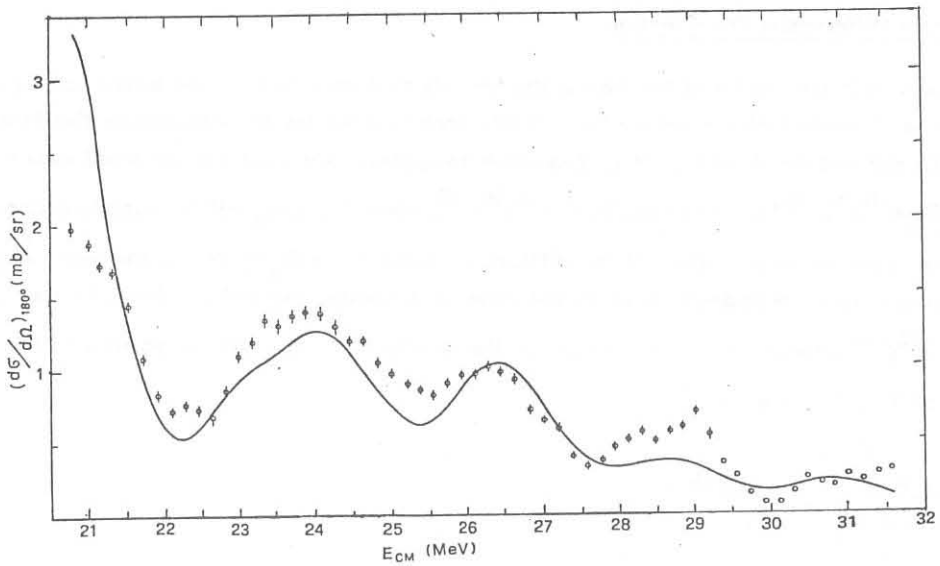

FIG. 4

However, the fit is hardly sensitive to the values of these parameters; in particular, a variation of θ_t by ≈ 0.35 rad does not appreciably change the fit. At energies higher than 31.5 MeV the fit fails. The experimental data oscillate more rapidly than the theoretical curve; moreover this latter decreases continuously at increasing energies, while the excitation function, after a rapid decrease between $\sim$ 32 and 40 MeV, raises again from $\sim$ 40 to 47 MeV. However, also at these energies some features of the excitation function can be understood, at least qualitatively, in the light of our model.

Firstly, if we observe the oscillations of the computer averaged excitation function (see Fig. 6 of Ref. (11)), we can verify that their frequency is still reproduced, with sufficient precision, by formula (41).

Secondly, we can do a number of considerations comparing the excitation functions of the elastic and inelastic scattering (see Fig. 4 of Ref. (11)). We distinguish among three different intervals:

a) from $\sim$ 32 to 40 MeV the elastic excitation function decreases rapidly, while the inelastic one raises;
b) from $\sim$ 40 to $\sim$47 MeV the elastic excitation function increases again, while the inelastic one is depressed;
c) from $\sim$ 47 to 52 MeV both the excitation functions go down rapidly and, after 50 MeV, the elastic one seems not to exhibit any structures at all.

Now we can try an explanation of these facts. It is reasonable to assume that the amplitude of the shortcut is attenuated by the inelastic channel; therefore, in the interval where the inelastic cross section increses, the shortcut contribution is strongly inhibites and the excitation function decreases exponentially; on the contrary, where the inelastic cross section is depressed, the amplitude of the shortcut is restored, and curves the raising and large oscillations of the excitation function. All that has some consequences also on the behaviour of the angular distribution. When the shortcut is inhibited, only the term p=0 is taken into account; therefore, since $\mathcal{P}_0(\xi_0^+)=1$, it is easy to see that formula (22), which we use to fit the backward angular distribution, holds true, not merely in a neighborhood of $\theta=\pi$, but in a larger angular interval. This is confirmed by our fit at energy E_{CM}=34.8 MeV (see Fig. 1): our theoretical function agree with the data in an angular region larger than the other fits. We expect also that at energies between 40 and 47 MeV we can extend our fits of the angular distributions only to a limited range, similarly to the sets at the lower energies. Lastly, the rapid decrease of both excitation functions after 47 MeV, without any more structures for $E_{CM} > 50$ MeV, could give an indication that new reaction channels open.

3.2. - Small Angle Differential Cross Section

As we have seen in the outline of the theory, the formula that we obtain for the diffracted ray contribution at small angles - i.e. formula (25) - is not useful in a fit. Therefore we try to approximate this formula by a more suitable one. To this end we show that it is reasonable to approximate - for not too small values of $(\theta_g - \theta)$ - the series $\sum_{n=1}^{\infty} D_n D'_n e^{-\alpha_a(\theta_g - \theta)}$ by a function like $C e^{-\alpha_a(\theta_g - \theta)}$, where C and α_a will be suitably defined in a moment. Since we do not know the exact values of the diffraction coefficients $D_n D'_n$ and of the decay exponents α_n, we verify the approximation mentioned above in the case of a neutral reflecting sphere. In this case the series $\sum_{n=1}^{\infty} D_n D'_n e^{-\alpha_n(\theta_g - \theta)}$ appears in the expression of the amplitude of the diffracted rays in the shadow region (formula (5.6) of Ref. (15), if we set[14]

$$D_n D'_n = \frac{e^{i\frac{\pi}{12}}}{2\sqrt{\pi}\, a'^2_n} \left(\frac{2}{\lambda_g}\right)^{1/6} \tag{45}$$

and

$$\alpha_n = \left(\frac{\lambda_g}{2}\right)^{1/3} x_n e^{-i\frac{\pi}{6}}, \tag{46}$$

where $-x_n$ is the n-th zero of the Airy function and

$$a'_n = A'_i(-x_n); \tag{47}$$

λ_g is the grazing angular momentum, $\lambda_g = kR$; $\theta_g = \arcsin\frac{r}{R}$.

To verify the approximation mentioned above, we insert (45) and (46) into the series $\sum_{n=1}^{\infty} D_n D'_n e^{-\alpha_n(\theta_g - \theta)}$ and consider the following succession of complex numbers:

$$S_j = \log\left[\sum_{n=1}^{\infty} D_n D'_n e^{-\alpha_n(\theta_g - \theta_j)}\right] \qquad \text{with} \qquad \theta_j = \frac{j-1}{20}\,\theta_g$$

for $j = 1, 2, \ldots, 20$.

Now we try a linear fit to this succession with the function

$$\mathcal{F}(\theta) = -\alpha_a \theta + c,$$

where we use α_a and c as free (complex) parameters; moreover we give λ_g and θ_g the six different values that we have found in our fits at fixed energies and at large angles. In this case we obtain fits whose variances are of the order of 10^{-2} as for the real part and of 10^{-4} for the imaginary part; only in the case corresponding to E_{CM}=21.1 MeV we have a slight discrepancy as regards the imaginary part, due to the large angular interval (nearly $\frac{\pi}{2}$ radians) that we consider. Moreover the values obtained for Re α_a and Im α_a are considerably larger than the corresponding values of Re α_1 and Im α_1, roughly they assume values which are intermediate with respect to Re α_1, Re α_2 ... Re α_N and to Im α_1, Im α_2 ... Im α_N, where N is the index at which we can truncate the series. Now we conjecture that our case is not very different from the one that we have just considered and therefore we assume that the above approximation can be extended to our case. In other words, we say that, in a phenomenological fit at fixed energy, formula (25) is practically indistinguishable from the following expression:

$$f_d(k,\theta) \approx \frac{e^{2i\Delta_g}}{\left[\cos\left(\frac{1}{2}\theta_g\right)\sin\theta\right]^{1/2}}\; e^{i\lambda_g(\theta_g - \theta)}\, C\, e^{-\alpha_a(\theta_g - \theta)}, \tag{48}$$

where $C = e^c$. Lastly we use the well-known expansion of $P_{\lambda-\frac{1}{2}}(\cos\theta)$, i.e. (see, e.g. Ref. (2))

$$P_{\lambda-\frac{1}{2}}(\cos\theta) \approx \frac{e^{-i\left(\lambda\theta - \frac{\pi}{4}\right)}}{(2\pi\lambda\sin\theta)^{1/2}} \qquad \left[\theta > (\mathrm{Im}\,\lambda)^{-1}\right]. \tag{49}$$

Substituting (49 into (48), we get formula (26), which is uniformly valid also in a neighborhood of θ=0. Therefore we can employ formula (27) to fit the data: we use B, γ and Im λ_a as free parameters, while we assign Re λ_a the same values found in the corresponding large angle fits. The fits are presented in Fig. 5 and the parameters are listed in Table II. The values of Im λ_a are considerably larger than the corresponding ones of Im λ_l deduced at large angles; a similar effect we had noted in π^+p elastic scattering[10]; also the values of Im λ_a found by Fuller and Moffa[2] in the small angle elastic cross section are very large That is not surprising, in the light of the

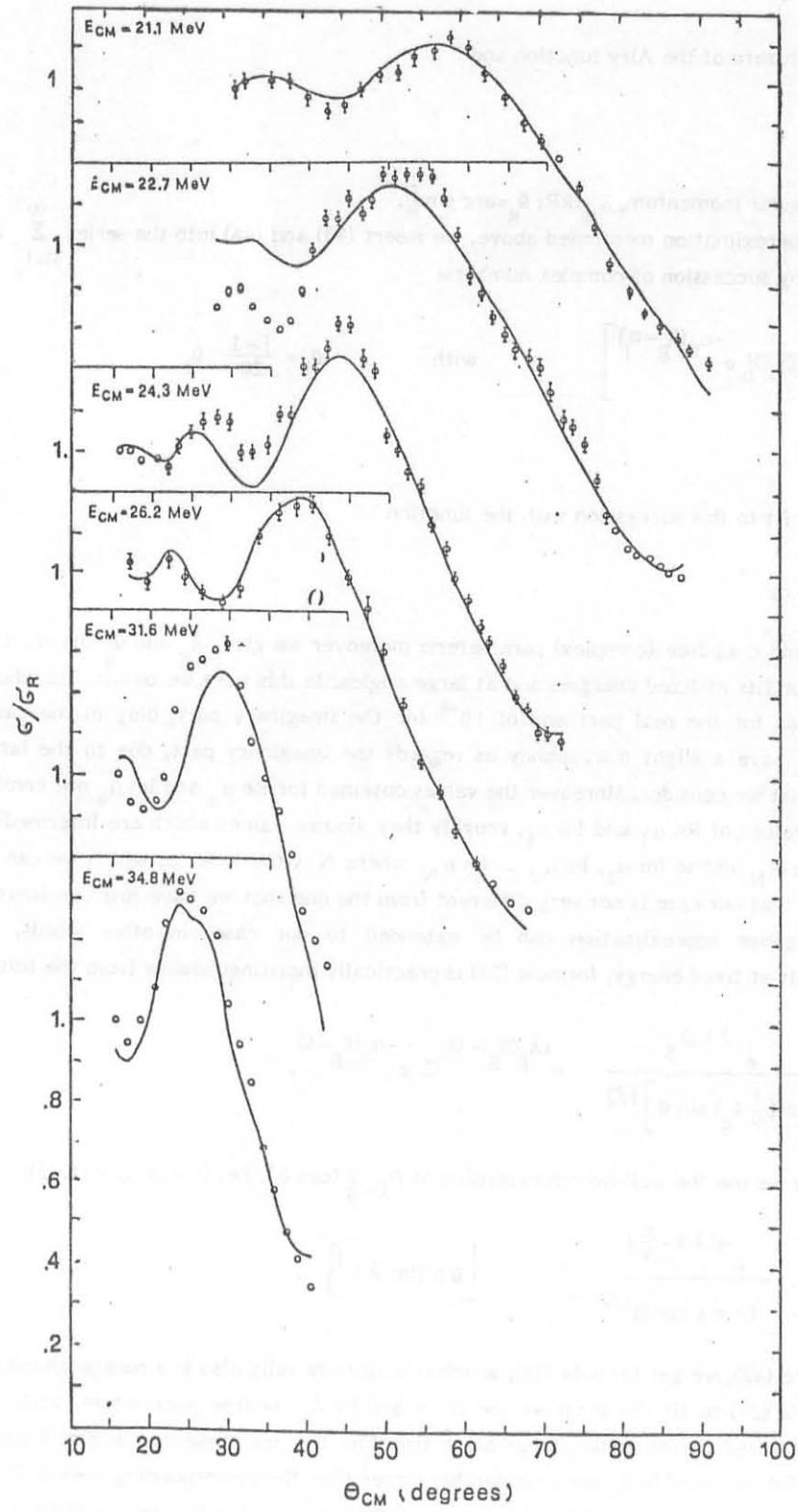
E_CM = 21.1 MeV
E_CM = 22.7 MeV
E_CM = 24.3 MeV
E_CM = 26.2 MeV
E_CM = 31.6 MeV
E_CM = 34.8 MeV
σ/σ_R
θ_CM (degrees)

FIG. 5

TABLE II - Values of the fit parameters, as obtained from the small angle fits to the $^{16}O+^{28}Si$ elastic scattering data at fixed energies.

E_{cm} (MeV)	$R \cdot B$ $[(mb/sr)^{\frac{1}{2}}]$	$Im\lambda_a$	γ	θ_g(deg)	θ_{max}(deg)
21.1	.264	2.65	2.400	93.47	86.3
22.7	.612	2.56	2.937	80.16	81.6
24.3	1.97	2.33	3.731	70.48	68.8
26.2	2.56	2.28	2.735	61.81	63.
31.6	3.44	3.61	.577	46.10	40.5
34.8	8.39	3.06	.338	40.14	39.

verification that we have done in the case of a neutral reflecting sphere: the values assumed by $Im\ \lambda_a = Re\ \alpha_a$ are intermediate with respect to $Re\ \alpha_1$, $Re\ \alpha_2$ ... $Re\ \alpha_N$, where N is the number at which the series can be truncated. Furthermore, as one can see from Table II, there is a strict correlation between the values assumed by θ_g (as calculated from formula (5)) and θ_{max}, which is the greatest angle at which we can extend the forward fit. Lastly the rapid increase of the coefficient B towards increasing energies can be understood qualitatively, if we observe formula (28): the exponential $e^{i\lambda_a\theta_g} = e^{i\lambda_g\theta_g} e^{-\alpha_a\theta_g}$ increases with energy, since θ_g is a decreasing function of the wave number. However a quantitative comparison between the formula and the values of the parameters is not possible, since we do not know the law of dependence of α_a and C on the energy.

We conclude this paragraph with an observation about the transition regions. As we have seen, these occur in neighborhoods of θ_g and of $\theta_t - \theta_g$. According to the value of θ_t and of θ_g that we have found, we can see that, at 21.1 MeV and at 22.7 MeV, $\theta_t - \theta_g$ is less than θ_g; so at angles between $\theta_t - \theta_g$ and θ_g we should take into account the contribution of the critically refracted rays and of those which take one shortcut. However the energies to which we refer do not support a fully asymptotic theory, moreover the edge of the interaction region is not neat; therefore it is not unreasonable to expect a smooth angular distribution, without any particular structures at $\theta = \theta_t - \theta_g$. Furthermore, since the term (26) (that describes the surface wave contribution for $\theta < \theta_g$) increases greatly as we move towards θ_g, and the two critical angles are sufficiently near to each other, we assume that this term is dominant over the shortcut contribution.

4. - CONCLUDING REMARKS

We can draw some conclusions from the above analysis.

1) The role of the surface waves in the elastic differential cross section is evident. This mechanism is to be preferred to the resonance model because of two facts.

a) The decay factor $Im\ \lambda_1$, which corresponds to the imaginary part of the location of a pole in the c.a.m. plane, is large ($Im\ \lambda_1 \gtrsim 0.6$), corresponding to a strong violation of the rotational symmetry; on the contrary a resonance is expected to be described by a pole whose imaginary part is very small ($Im\ \lambda_1 \lesssim 0.01$), so that the rotational symmetry is hardly broken. Furthermore $Im\ \lambda_1$ varies slowly with energy, exhibiting a trend

similar to that of the poles - to be interpreted as surface waves - of the Debye expansion of the S-function for the scattering of a plane wave by a trasparent sphere[16].

b) The angular distribution at backwards behaves in the same way at all the energies, whereas a resonance model provides that the large angle differential cross section is different according as we are near to a resonant energy or far from it.

In this connection it is worth mentioning some authors who, starting from optical potentials which fit the elastic-scattering data of $^{16}O+^{28}Si$, analize the scattering amplitude in terms of semiclassical S-matrix elements[20]. Anni et al.[17] and Lee[20] conclude that ALAS in $^{16}O+^{28}Si$ is dominated by a surface wave effect.

2) Also the reflected ray contribution at large angles has been made evident. In this connection we wish to stress that, as regards the reflection amplitude, we have not introduced any new parameters in the fit to the excitation function at $\theta = \pi$, but we have just used the parameters extracted from the fits at fixed energies. It is properly the reflection amplitude which, interfering with the surface rays, produces the first two oscillations in the excitation function, in agreement with the experimental data (see Fig. 4).

3) The trend of the excitation function is consistent with a shortcut mechanism, which can occur only if a nearly transparent shell surrounds the opaque core. In this connection we conjecture that, as in the case of α-^{40}Ca elastic scattering, the observed isotope effect could be due to a different behaviour of the inelastic and reaction channels at large angular momenta, according as the colliding nuclei have closed shells or not. We think that a possible correlation between the magnitude of the large angle peak and the density of states of the reaction channels open should be cheked, similarly to what was done in the case of α-Nuclei collisions[21].

4) Lastly, we prefer to explain the forward angular distribution as a diffractive effect, rather than as a refractive one ("rainbow" [22]), since the edge of the nuclear potential is rapidly varying, as our analysis at large angles seems to confirm.

ACKNOWLEDGEMENTS

The author is grateful to Prof. G.A. Viano for many useful discussions and suggestions. Moreover he thanks Prof. P. Braun-Munzinger for having kindly sent him the numerical data used in the fits and for a stimulating discussion during the Varenna School.

REFERENCES

(1) E. Di Salvo and G.A. Viano, Nuovo Cimento A, to be published.
(2) R.C. Fuller and P.J. Moffa, Phys. Rev. C15, 266 (1977).
(3) J. Barrette, M.J. Le Vine, P. Braun-Munzinger, G.M. Berkowitz, M. Gai, J.W. Harris and C.M. Jachcinski, Phys. Rev. Letters 40, 445 (1978).
(4) D. Dehnhard, V. Shkolnik and M.A. Franey, Phys. Rev. Letters 40, 1549 (1978); M.A. Franey, V. Shkolnik and D. Denhard, Phys. Letters 81B, 139 (1979).
(5) S. Kubono, P.D. Bond, D. Horn and C.E. Thorn, Phys. Letters, 84B, 408 (1979).
(6) S.Y. Lee, Nuclear Phys. A311, 518 (1978).
(7) S. Kahana, B.T. Kim and M. Mermaz, Phys. Rev. C20, 2124 (1979).
(8) W.E. Frahn, Phys. Rev. Letters 26, 568 (1977).
(9) E.J. Williams, Rev. Mod. Phys. 17, 217 (1945).
(10) E. Di Salvo and G.A. Viano, Nuovo Cimento A59, 11 (1980).
(11) P. Braun-Munzinger, G.M. Berkowitz, M. Gai, C.M. Jachcinski, T.R. Renner and C.D. Uhlhorn, Phys. Rev. C24, 1010 (1981).
(12) R. Anni, L. Renna and L. Taffara, Nuovo Cimento A55, 456 (1980).
(13) J.G. Cramer, R.M. De Vries, D.A. Goldberg, M.S. Zisman and C.F. Maguire, Phys. Rev. C14, 2158 (1976).
(14) B.R. Levy and J.B. Keller, Comm. Pure Appl. Math. 12, 159 (1959).
(15) H.M. Nussenzveig, Ann. Phys. 34, 23 (1965).
(16) H.M. Nussenzveig, J. Math. Phys. Phys. 10, 85 (1969).
(17) R. Anni, L. Renna and L. Taffara, Lett. Nuovo Cimento 25, 121 (1979).
(18) T. Takemasa and T. Tamura, Phys. Rev. C18, 1282 (1978).
(19) S. Landowne, Phys. Rev. Letters 42, 633 (1979).
(20) S.Y. Lee, Nuclear Phys. A311, 518 (1978).
(21) J.S. Eck, W.J. Thompson, K.A. Ebherard, J. Schiele and W. Trombik, Nuclear Phys. A255, 157 (1975).
(22) R. Da Silveira, Phys. Letters 45B, 211 (1973).